Nanotechnology

Size-tunable MRI-visible nitroxide-based magnetic mixed micelles: preparation, stability, and theranostic application

To cite this article before publication: Kota Nagura *et al* 2019 *Nanotechnology* in press https://doi.org/10.1088/1361-6528/ab0627

Size-Tunable MRI-Visible Nitroxide-Based Magnetic Mixed Micelles: Preparation, Stability and Theranostic Application

Kota Nagura[1], Alexey Bogdanov[2], Natalia Chumakova[2], Andrey Kh. Vorobiev[2], Satori Moronaga[1], Hirohiko Imai[3], Tetsuya Matsuda[3], Yohei Noda[4], Tomoki Maeda[4], Satoshi Koizumi[4], Koichi Sakamoto[5], Tsukuru Amano[6], Fumi Yoshino[6], Tatsuhisa Kato[1], Naoki Komatsu*[1], Rui Tamura*[1]

[1]Graduate School of Human and Environmental Studies, Kyoto University, Kyoto 606-8501, Japan
[2]Department of Chemistry, M.V. Lomonosov Moscow State University, Moscow 119991, Russian Federation
[3]Graduate School of Informatics, Kyoto University, Kyoto 606-8501, Japan
[4]Institute of Quantum Beam Science, Ibaraki University, Ibaraki 316-8511, Japan
[5]DKS Co. Ltd., Kyoto 600-8873, Japan
[6]Department of Obstetrics and Gynecology, Shiga University of Medical Science, Shiga 520-2192, Japan

Abstract

Metal-free magnetic mixed micelles (mean diameter: 16 nm) composed of biocompatible surfactant Tween 80 and hydrophobic pyrrolidine-*N*-oxyl radical were prepared by mixing them in phosphate-buffered saline (PBS). The magnetic mixed micelles were characterized by dynamic light scattering (DLS) and small angle neutron scattering (SANS) measurements. The stability of the micelles is found to depend on the length of alkyl side chain in the nitroxide compounds and degree of unsaturation in the hydrophobic chain in the surfactant. The size of the mixed micelle can be tuned by changing the molar ratio of Tween 80 and nitroxyl radical. In view of theranostic application of the micelle, the cytotoxicity and stability in a physiological environment was investigated; the mixed micelle exhibited no cytotoxicity, high colloidal stability and high resistance towards reduction by large excess ascorbic acid. The *in vitro* and *in vivo* magnetic resonance imaging (MRI) revealed sufficient contrast enhancement in the proton longitudinal relaxation time (T_1) weighted images. In addition, hydrophobic fluorophores and an anticancer drug are stably encapsulated in the mixed micelles and showed fluorescence (FL) upon reduction by ascorbic acid and cytotoxicity to cancer cells, respectively. For example, the paclitaxel-loaded mixed micelles efficiently suppressed cancer cell growth. Furthermore, they were found to give higher MRI contrast (higher r_1 value) *in vitro* than the micelles without paclitaxel. The magnetic mixed micelles presented here are promising theranostic agents in nanomedicine due to their high biocompatibility and high resistivity towards reduction as well as functions as drug carrier in therapy and MR or FL imaging probe in diagnosis.

I. Introduction

Magnetic resonance imaging (MRI) is one of the most frequently used imaging techniques in clinical medicine, and MRI contrast agents are sometimes required for more accurate diagnosis. Gadolinium (III) (Gd^{3+}) complexes such as Magnevist are widely used as paramagnetic metal ion-based contrast agents for MRI [1-3]. However, the patients with impaired kidney function face a risk of a serious adverse reaction termed nephrogenic systemic fibrosis (NSF) by using Gd^{3+} contrast agents [4,5]. Since the first report of this adverse effect on renal dialysis patients, guidelines for the administration of Gd^{3+} contrast agents have been issued and implemented worldwide to minimize the risk of NSF [6,7]. Since then, metal-free materials including nitroxide radical compounds have been investigated as proton longitudinal relaxation time (T_1) enhancing agents [8-10].

Nitroxide radicals have attracted great interest as a relatively safe spin source for several decades despite the lower contrast ability than Gd^{3+} complex, because the sterically protected N-O group is thermally stable in the air. A polymer-based nanoparticle composed of nitroxide lipids and glycerol monooleate was recently reported by Muir and co-workers as an MRI contrast agent [11]. However, the mean diameters (> 180 nm) were too large to have passive targeting property based on enhanced permeation and retentive effect in cancer therapy and diagnosis. Although the spirocyclohexyl nitroxide polyradicals based on branched-bottlebrush copolymers and the polypropylenimine dendrimer scaffolds were also reported, the functions of these materials were limited to MRI contrast [12,13]; no other functions such as drug carrier nor fluorescence (FL) imaging were endowed.

In this context, we prepared the metal-free 'magnetic mixed micelles' (the term 'nanoemulsions' was used in ref. 14) comprised of equimolar amounts of polyoxyethylene (20) cetyl ether (Brij58, **1**) and (±)-2,2,5-trimethyl-5-(4-alkoxyphenyl) pyrrolidine-*N*-oxyl radical ($\mathbf{2}_n$) according to a simple experimental protocol [14]. These micelles showed high colloidal stability, high resistance to a reducing agent, and enough contrast enhancement in the T_1-weighted MRI in PBS *in vitro*. In addition, fluorophores or a drug was stably encapsulated inside the mixed micelles. However, the surfactant **1** exhibited cytotoxicity in 0.16 μM or higher, while nitroxide radials such as $\mathbf{2}_n$ are generally known to show very low toxicity to cells and animals [15-18]. Therefore, we focused on the surfactant 'Tween 80 and 60' (**3** and **4**, respectively), because they have been employed in clinical medicine owing to their biocompatibility [19-21]. Here we report the preparation, stability and theranostic application of the magnetic mixed micelles composed of surfactant Tween 80 (**3**) and nitroxide radical ($\mathbf{2}_{18}$) as well as the micelles including fluorophores and a drug.

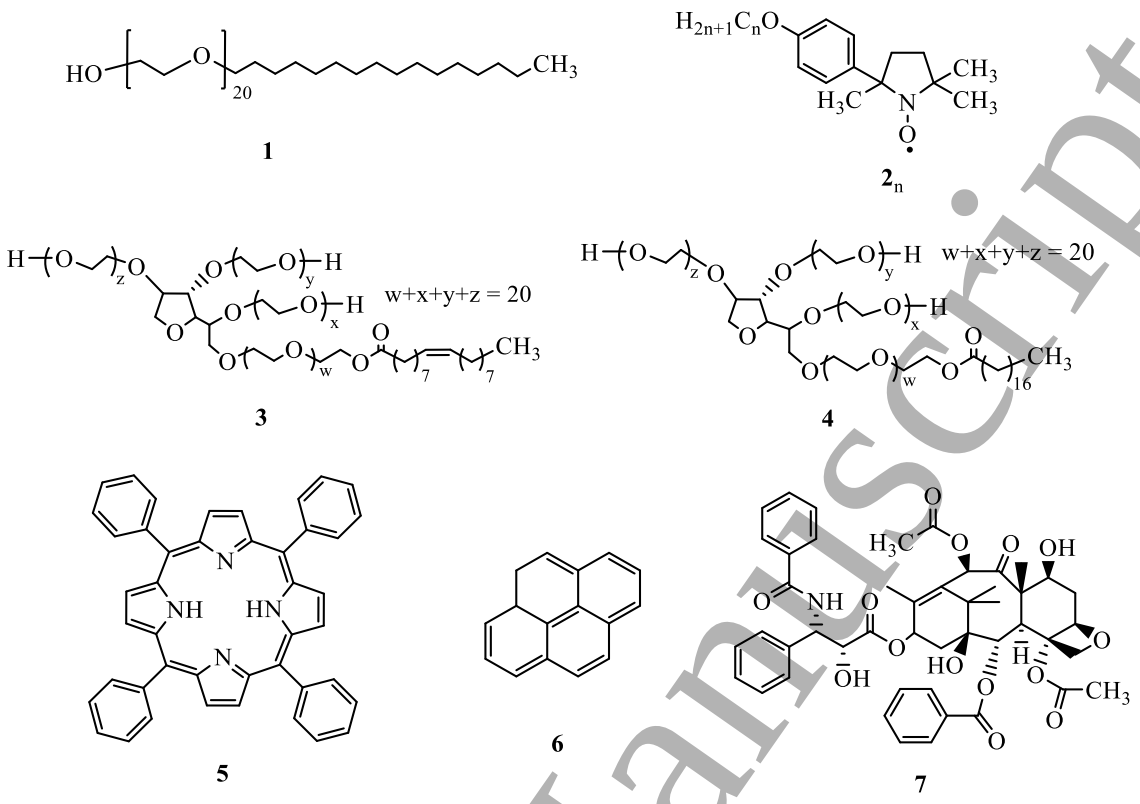

Figure 1. Molecular structures of non-ionic surfactant Brij58 (**1**), nitroxide radicals [$\mathbf{2}_n$ (n = 12, 14, 16, 18 and 20)], Tween 80 (**3**), Tween 60 (**4**), tetraphenylporphyrin (**5**), pyrene (**6**), and paclitaxel (**7**).

II. Results and Discussion

II-1. Preparation and Stability

II-1-1. Preparation and stability of magnetic mixed micelles of 3/2$_n$ and 4/2$_n$

The mixed micelles composed of **3** and $\mathbf{2}_n$, and **4** and $\mathbf{2}_n$ (Figure 1), designated as **3**/$\mathbf{2}_n$ and **4**/$\mathbf{2}_n$ respectively, were prepared at concentration of 10 mM in phosphate buffer saline (PBS) according to the experimental procedure described in the Supplementary Information.

The stability of the micelles was found to depend on the length of the alkyl chain (n = 12, 14, 16, 18 and 20) in the radical $\mathbf{2}_n$ and the degree of unsaturation in the hydrophobic chain in the surfactants **3** and **4** (Figure 1). **3**/$\mathbf{2}_{18}$ was formed as a clear yellow dispersion immediately after preparation and the appearance did not change for one month (Table 1). Although the micelles of **3** with **2** (**3**/$\mathbf{2}_{16}$ and **3**/$\mathbf{2}_{20}$) having shorter and longer alkyl chains than $\mathbf{2}_{18}$ also gave clear yellow solution immediately after preparation, they were unstable to give white precipitates within one month. The radicals **2** ($\mathbf{2}_{12}$ and $\mathbf{2}_{14}$) with alkyl chains shorter than $\mathbf{2}_{16}$ precipitated within 24 h after mixing with **3**. These observations for **3**/$\mathbf{2}_n$ clearly indicate that the most appropriate chain length (n) in $\mathbf{2}_n$ is 18, probably because of a similar length to that of the hydrophobic part of **3** (n = 17) [14]. However, the stability of the mixed micelles decreased significantly, when the alkenyl group with the *cis*-

configuration in **3** was replaced by saturated C_{17} alkyl chain in **4**. That is, **4/2**$_{16}$, **4/2**$_{18}$ and **4/2**$_{20}$ were less stable, and **4/2**$_{12}$ and **4/2**$_{14}$ were much less stable than **3/2**$_{18}$. This significant stability difference between **3/2**$_{18}$ and **4/2**$_{18}$ may be caused by the difference in the chain length and/or rigidity due to the C = C with *cis*-configuration. The CH/π interaction is also conceivable to increase the intermolecular interaction other than the hydrophobic one. From these observations shown in Table 1, the order of the stability in the micelles **3/2**$_n$ and **4/2**$_n$ is concluded to be **3/2**$_{18}$ > **3/2**$_{16}$, **4/2**$_{16}$, **4/2**$_{18}$, **3/2**$_{20}$ and **4/2**$_{20}$ > **3/2**$_{14}$, **4/2**$_{14}$, **3/2**$_{12}$ and **4/2**$_{12}$.

Table 1. Mean diameters and colloidal stability of the mixed micelles **3/2**$_n$ and **4/2**$_n$ (n = 12 – 20) in PBS at 30 °C.

		2$_{12}$ and **2**$_{14}$	**2**$_{16}$	**2**$_{18}$	**2**$_{20}$
3	Diameter by DLS	—	18 nm[a]	16 nm[a]	22 nm[a]
	Observation	precipitates[a]	solution[a] → precipitates[b]	solution[a] → solution[b]	solution[a] → precipitate[b]
4	Diameter by DLS	—	21 nm[a]	17 nm[a]	58 nm[a]
	Observation	precipitates[c]	solution[a] → precipitates[c]	solution[a] → precipitates[c]	solution[a] → precipitates[c]

[a]Immediately after preparation (Figure S1). [b]One month after preparation. [c]One day after preparation.

After preparation of the mixed micelles, mean diameters of the resulting magnetic mixed micelles (**3/2**$_n$ and **4/2**$_n$, n = 16, 18 and 20) in PBS were measured by dynamic light scattering (DLS) and small angle neutron scattering (SANS) analyses. The mean diameter of **3/2**$_{18}$ was 16 nm (100% in in Figure 2a) even after the 1000-fold dilution (to 0.01 mM) with PBS, supporting the above conclusion of the high stability in **3/2**$_{18}$. In addition, the size of **3/2**$_{18}$ is the smallest among the micelles (**3/2**$_n$ and **4/2**$_n$, n = 16, 18 and 20) (Table 1, Figure S1). The mean diameter (16 nm) of **3/2**$_{18}$ by DLS in PBS was also supported by SANS measurement in D_2O; the SANS profile observed at iMATERIA (BL20, J-PARC) was in good agreement with the scattering function for spherical particles. The mean diameter is estimated to be 14 nm which is slightly smaller than that (16 nm) determined by DLS (Figure S3 and S4). This deviation can be explained by the difference in the principle of these analyses; light and neutron scattering. Because DLS is based on hydrodynamics of micelle diffusion, the determined diameter of the **3/2**$_{18}$ reflects the whole micelle size including water. In contrast, SANS observes scattering length density difference (contrast) between the micelle and surrounding medium.

The weak SANS contrast in the hydrophilic corona region including D_2O is considered to make the diameter of **3**/$\mathbf{2}_{18}$ to be smaller than that by DLS [22].

When the molar ratio was changed in the preparation of the mixed micelles **3**/$\mathbf{2}_{18}$ containing 0 – 100 mol% of $\mathbf{2}_{18}$ in PBS, the diameter of the resulting micelle was found to be proportional to the molar content of $\mathbf{2}_{18}$ as shown in Figure 2. This indicates that the size of the mixed micelle can be tuned by changing the molar ratio of **3** and $\mathbf{2}_{18}$; for example, 16 and 11 nm diameters for 1 / 1 and 9 / 1 molar ratio, respectively.

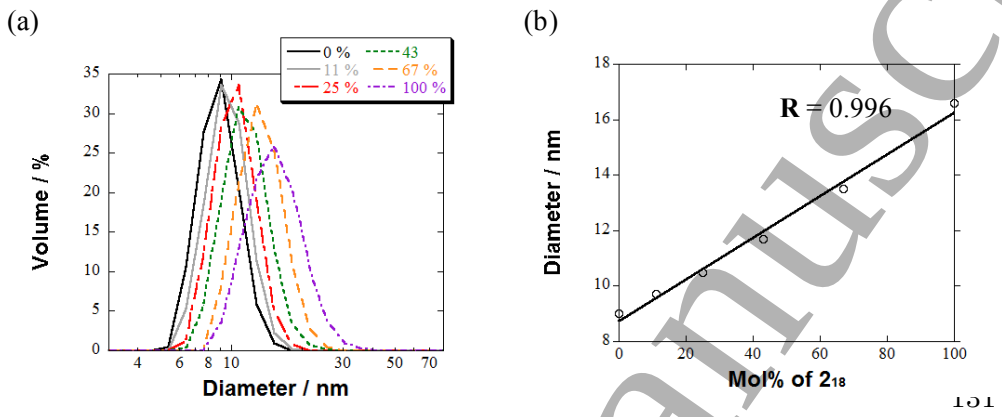

Figure 2. (a) The dependence of the mol% of $\mathbf{2}_{18}$ in **3**/$\mathbf{2}_{18}$ on the mean diameters by DLS at 25 °C in PBS (mol% of $\mathbf{2}_{18}$ = 0, black solid line; 11, gray solid line; 25, red long-broken line; 43, green dotted line; 67, orange short-broken line; 100, purple broken dotted line). (b) Proportional relationship between the mol% of $\mathbf{2}_{18}$ in **3**/$\mathbf{2}_{18}$ and mean diameters of **3**/$\mathbf{2}_{18}$.

II-1-2. Preparation and stability of magnetic mixed micelles of 3/2_{18}/X (X = 5, 6 or 7)

The micelles of **3**/$\mathbf{2}_{18}$ including fluorophore (**5** or **6**) or drug (**7**), designated as **3**/$\mathbf{2}_{18}$/**X** (**X** = **5**, **6** or **7**), were prepared by adding **5** (1.0 mol%), **6** (10 mol%), or **7** (10 mol%) upon the preparation of **3**/$\mathbf{2}_{18}$. The experimental detail is described in the Supplementary Information. The incorporation of **5** and **6** into the mixed micelles was confirmed by FL quenching (Figure 3), which is known to be caused by surrounding nitroxide radicals [23-27]. However, the FL was revived by adding a large excess (20 equiv based on $\mathbf{2}_{18}$) of ascorbic acid as a reducing agent in both **3**/$\mathbf{2}_{18}$/**X** (**X** = **5** and **6**). As shown in Figure 3, the intensity of FL started to increase, when the amount of radical monitored by EPR spectroscopy became less than half at around 30 min. These phenomena can be interpreted by reduction of the nitroxide radicals to *N*-hydroxy groups which cannot quench the fluorophores.

The mean diameter (11 nm) of **3**/$\mathbf{2}_{18}$/**7** was smaller than those of **3**/$\mathbf{2}_{18}$, **3**/$\mathbf{2}_{18}$/**5** and **3**/$\mathbf{2}_{18}$/**6** (16, 14 and 15 nm, respectively, in Figure S2). **3**/$\mathbf{2}_{18}$/**7** was found to be more stable than **3**/$\mathbf{2}_{18}$/**5** and **3**/$\mathbf{2}_{18}$/**6**, based on the observation that **3**/$\mathbf{2}_{18}$/**7** was dispersed stably more than one month, while the micelles of **3**/$\mathbf{2}_{18}$/**5** and **3**/$\mathbf{2}_{18}$/**6** collapsed within one month giving white precipitates.

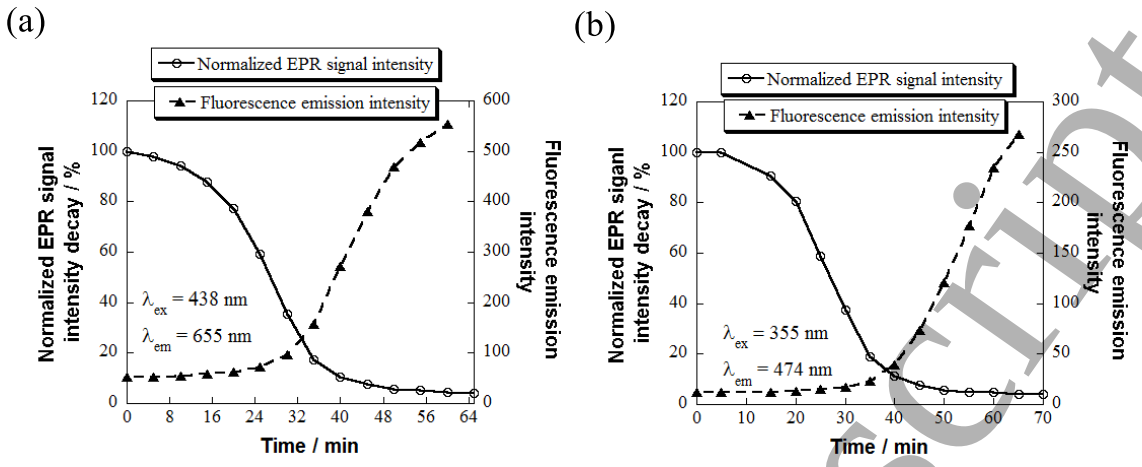

Figure 3. FL intensity change after addition of 20 equiv of ascorbic acid to (a) **3**/$\mathbf{2}_{18}$/**5** and (b) **3**/$\mathbf{2}_{18}$/**6** at 25 °C in PBS. The decrease and increase in the spectral intensity were monitored by EPR spectroscopy using a double-integration method and FL spectroscopy, respectively. See the Supplementary Information for experimental details.

II-1-3. Stability of magnetic mixed micelles in the presence of reducing agent

Ascorbic acid exists *in vivo* in concentration from μM to mM depending on the type of tissue. When nitroxide radicals are applied to *in vivo* MRI, they are known to be reduced to the diamagnetic hydroxylamines by ascorbic acid, resulting in significantly weakening the MRI contrast [28-30]. For example, TEMPOL, one of the most typical water-soluble nitroxide radical, is reduced quickly to hydroxylamine in the presence of ascorbic acid [14,31-36]. In our molecular design, four long hydrophilic tails in **3** and four neighboring substituents in $\mathbf{2}_{18}$ are expected to enhance resistance to ascorbic acid sterically. The decay of $\mathbf{2}_{18}$ in **3**/$\mathbf{2}_{18}$ in the presence of a large excess (20 equiv based on $\mathbf{2}_{18}$) of ascorbic acid in PBS was monitored by EPR spectroscopy (Figure 4). The result was compared with that of **1**/$\mathbf{2}_{18}$. As expected, **3**/$\mathbf{2}_{18}$ showed much higher resistance ($t_{1/2}$ = 33 min) than those of **1**/$\mathbf{2}_{18}$ ($t_{1/2}$ = 7 min) and TEMPOL ($t_{1/2}$ < 1 min). This is because ascorbic acid was likely to be trapped by three hydrophilic polyethylene glycol (PEG) chains in **3** more tightly than single PEG chain in **1**; ascorbic acid was prevented from invading into **3**/$\mathbf{2}_{18}$ more efficiently than **1**/$\mathbf{2}_{18}$. Similarly, the resistivity of the nitroxide radical in **1**/$\mathbf{2}_{18}$/**7** and **3**/$\mathbf{2}_{18}$/**7** was evaluated (Figure 4). As a result, **1**/$\mathbf{2}_{18}$/**7** and **3**/$\mathbf{2}_{18}$/**7** showed much higher resistance ($t_{1/2}$ = 64 min each) than the **1**/$\mathbf{2}_{18}$ ($t_{1/2}$ = 7 min) and **3**/$\mathbf{2}_{18}$ ($t_{1/2}$ = 33 min) did. These results imply that the structure of **3**/$\mathbf{2}_{18}$/**7** is different from those of **3**/$\mathbf{2}_{18}$, **3**/$\mathbf{2}_{18}$/**5** and **3**/$\mathbf{2}_{18}$/**6**. We believe that these contrast agents have enough stability even in the reducing microenvironment of tumor on the tumor targeting *in vivo* MRI.

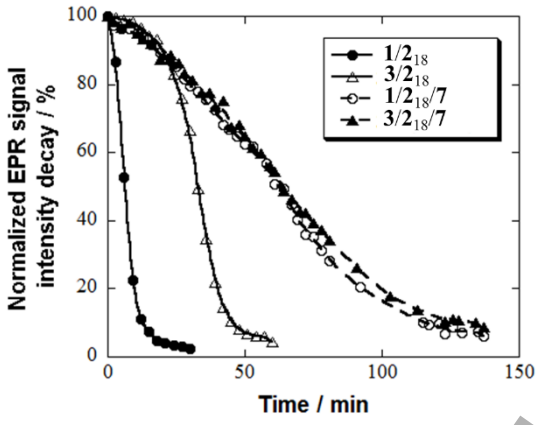

Figure 4. Comparison of the reduction resistance to a large excess of ascorbic acid among **1**/**2**$_{18}$, **3**/**2**$_{18}$, **1**/**2**$_{18}$/**7** and **3**/**2**$_{18}$/**7**. The reduction of the radical was monitored by EPR spectroscopy using a double-integration method. See the Supplementary Information for experimental details.

II-2. Theranostic Appplication

II-2-1. In vitro cytotoxicity of magnetic mixed micelles against HeLa cell

Since biocompatibility is a prerequisite for a magnetic mixed micelle as an MRI contrast agent, the cancer cell viability of **3**/**2**$_{18}$ was assessed and compared with that of **1**/**2**$_{18}$ by the CCK-8 assay at the initial concentrations of 2.5 mM for **1**, **3** and **2**$_{18}$ (Figure 5a). **3**/**2**$_{18}$ exhibited no significant cytotoxicity to HeLa cells at concentrations up to 2.5 mM, whereas **1**/**2**$_{18}$ showed cytotoxicity at 0.31 mM or higher, demonstrating that **3**/**2**$_{18}$ is more appropriate than **1**/**2**$_{18}$ for *in vivo* applications. In contrast, **3**/**2**$_{18}$/**7** with the ratio of 1 : 1 : 0.001 at the initial concentrations of 2.5 mM for **3** and **2**$_{18}$, and 2.5 μM for **7** displayed significant toxicity in 0.16 μM or higher of **7** as with free **7** (Figure 5b). Thus, these results suggest that **3**/**2**$_{18}$/**7** is incorporated into the HeLa cells and can be used as an MRI-visible DDS drug carrier.

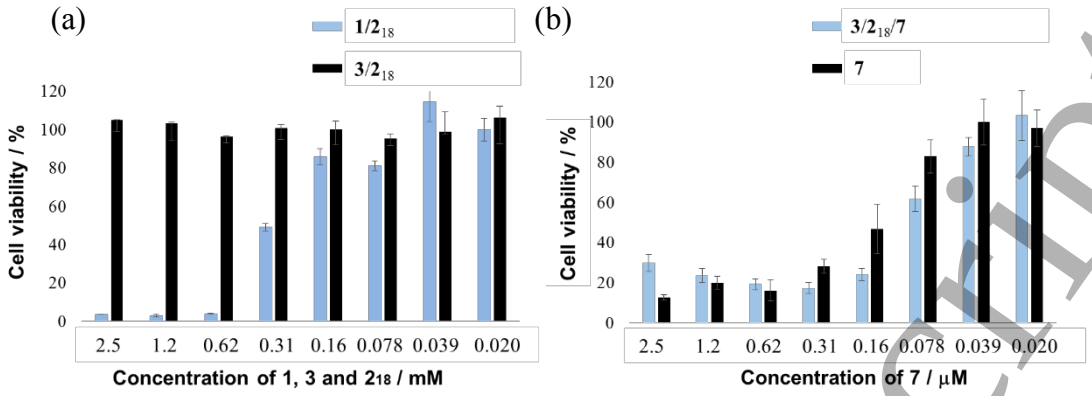

193 **Figure 5**. Comparison of the *in vitro* cytotoxicity between (a) **1**/**2**$_{18}$ and **3**/**2**$_{18}$, and (b) **3**/**2**$_{18}$/**7** and free
194 **7** by using Hela cells. The cell viability was assayed by using the CCK-8 kit after incubation for 24 h
195 at 37 °C under 5% CO_2. See the Supplementary Information for experimental details.
196
197 ***II-2-2. MRI measurement***
198 The longitudinal relaxivity (r_1) of **3**/**2**$_{18}$ was determined from relaxation time (T_1) as a function of
199 concentration at 25 °C and compared with that of **1**/**2**$_{18}$ (Figure 6). The T_1 values for the two magnetic
200 mixed micelles (1.2 – 10 mM for each component) in PBS were evaluated by using an MRI machine
201 at 7.0 T. Sufficiently bright T_1-weighted MR phantom images were obtained at a concentration of 10
202 mM for both magnetic mixed micelles, compared with PBS (Figure 6a, Panel A and E), indicating that
203 **3**/**2**$_{18}$ can be used as an MRI contrast agent *in vivo* in this concentration or higher [14]. Linear
204 regression analysis yielded r_1 = 0.07 $mM^{-1}s^{-1}$ for **3**/**2**$_{18}$ and r_1 = 0.09 $mM^{-1}s^{-1}$ for **1**/**2**$_{18}$ (Figure 6b).
205 These r_1 values were less than that (3.4 $mM^{-1}s^{-1}$) of Magnevist (a Gd^{3+} complex agent) in deionized
206 water [2]. However, this result is quite natural because **2**$_{18}$ with only one unpaired electron (S = 1/2)
207 should show inferior water proton relaxivity to Gd^{3+} (S = 7/2).
208

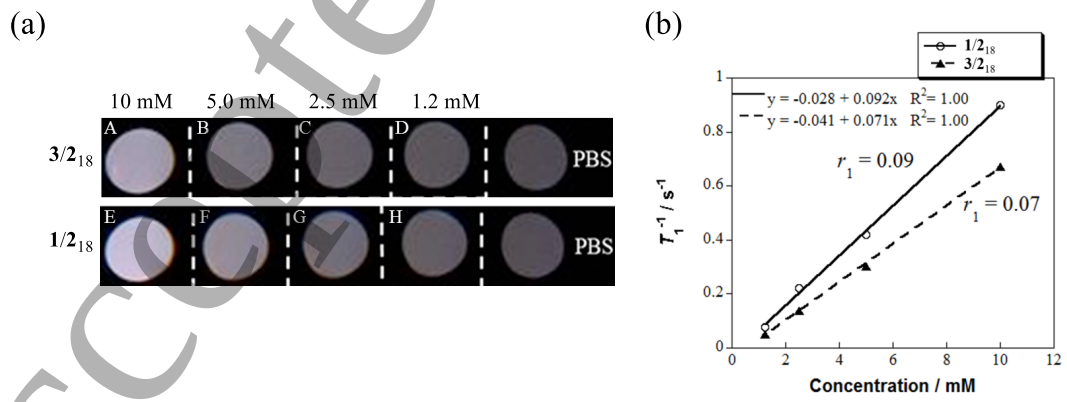

209
210 **Figure 6**. (a) T_1-weighted MR phantom images (7.0 T, 25 °C) of (A) – (D) **3**/**2**$_{18}$ and (E) – (H) **1**/**2**$_{18}$ at
211 1.2, 2.5, 5.0 and 10 mM in PBS, and PBS as control. (b) Plots of T_1^{-1} vs the concentrations of **3**/**2**$_{18}$

(broken line) and **1**/**2**$_{18}$ (solid line) in the magnetic mixed micelles to determine the r_1 values. See the Supplementary Information for experimental details.

Interestingly, **3**/**2**$_{18}$/**7** exhibited brighter MRI contrast (Figure 7a) and the larger r_1 value (r_1 = 0.14 mM^{-1}s^{-1}) than those (r_1 = 0.06 and 0.07 mM^{-1}s^{-1}) of **3**/**2**$_{18}$/**5** and **3**/**2**$_{18}$/**6**, respectively (Figure 7b). These experimental results can be interpreted by the reduced rotation diffusion of **2**$_{18}$ inside the mixed micelles [37–41]. In order to estimate the rotation diffusion mobility of the radicals, the EPR spectra of the mixed micelles of **3**/**2**$_{18}$ with the ratio of 1 : 0.01 and those including 10 mol% of **7** (**3**/**2**$_{18}$/**7** with the ratio of 1 : 0.01 : 0.1) in the temperature range of 263 to 313 K were numerically simulated as described in the Supplementary Information (Figure 8 and S5). The rotation diffusion tensor of the radical in **2**$_{18}$ in all investigated micelles has axial symmetry. The rotation diffusion coefficient D_z is within the range (1 – 10) × 10^8 s^{-1} (Table S1), but the values D_x and D_y are less than 2 × 10^6 s^{-1}. The temperature-dependence of the rotation diffusion mobility is successfully described by Arrhenius law with values of activation energy (E^a_z) shown in Table 2, indicating that **7** makes the mixed micelles more rigid to give enhanced MRI signal.

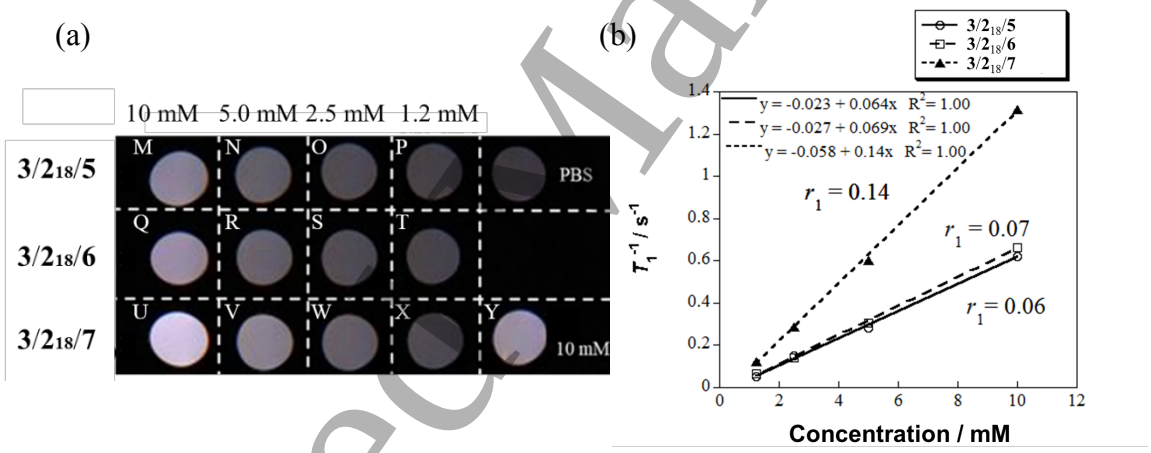

Figure 7. (a) T_1-weighted MR phantom images (7.0 T, 25 °C) of (M – P) **3**/**2**$_{18}$/**5**, (Q – T) **3**/**2**$_{18}$/**6**, and (U – X) **3**/**2**$_{18}$/**7**, at 1.2, 2.5, 5.0 and 10 mM in PBS, PBS as control, and **3**/**2**$_{18}$ (equimolar mixture) (10 mM each) (Y). (b) Plots of T_1^{-1} vs the concentrations of **3**/**2**$_{18}$ in the **3**/**2**$_{18}$/**5** (solid line), **3**/**2**$_{18}$/**6** (broken line) and **3**/**2**$_{18}$/**7** (dotted line) to determine the r_1 values.

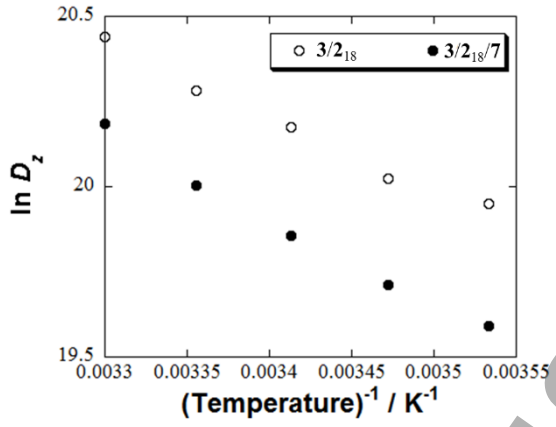

Figure 8. Temperature dependence of rotation diffusion coefficient *Dz* of **2**$_{18}$ in **3**/**2**$_{18}$ with the ratio of 1 : 0.01 and **3**/**2**$_{18}$/**7** with the ratio of 1 : 0.01 : 0.1. See the Supplementary Information for experimental details.

Table 2. The effective activation energy of rotation diffusion of **2**$_{18}$ in **3**/**2**$_{18}$ with the ratio of 1 : 0.01 and **3**/**2**$_{18}$/**7** with the ratio of 1 : 0.01 : 0.1.

Mixed micelle	E^a_z / kJ/mol
3/**2**$_{18}$	18.4 ± 0.4
3/**2**$_{18}$/**7**	22.9 ± 0.6

Finally, the magnetic mixed micelle **3**/**2**$_{18}$ was applied to *in vivo* MRI in mice. The experimental details are described in the Supplementary Information. As shown in Figure 9, distinct MRI contrast enhancement with high reproducibility was observed in the liver after injection. This result demonstrates that the magnetic mixed micelles are effective as an *in vivo* T_1-weighted MRI contrast agent.

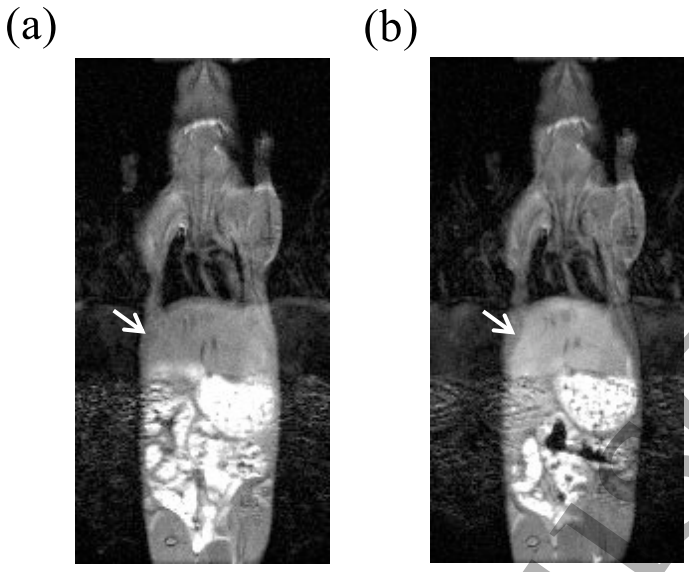

Figure 9. Coronal T_1-weighted MR images of the liver of a male ICR mouse: (a) before and (b) 23 min after the intravenous injection of 200 μL of **3**/**2**$_{18}$ in PBS. Distinct contrast enhancement was observed in the liver (indicated by white arrows). See the Supporting Information for experimental details.

Conclusions

We have prepared highly robust, size-tunable and biocompatible metal-free magnetic mixed micelles **3**/**2**$_{18}$. The guest-unloaded magnetic mixed micelles **3**/**2**$_{18}$ showed lower cytotoxicity, high colloidal stability and higher reduction resistance to a large excess of ascorbic acid, compared with previously reported magnetic mixed micelles **1**/**2**$_{18}$ [14]. In addition, **3**/**2**$_{18}$ demonstrated sufficient contrast enhancement in the T_1 weighted MR images *in vitro* and *in vivo*.

Furthermore, the mixed micelle encapsulated a hydrophobic drug of paclitaxel (**7**) (10 mol %), or hydrophobic fluorophores of tetraphenylporphyrin (**5**) (1.0 mol%) and pyrene (**6**) (10 mol%) to give stable micelles with mean particle sizes of less than 20 nm. The **7**-loaded magnetic mixed micelles, **3**/**2**$_{18}$/**7**, effectively suppressed HeLa cell growth. Thus, such highly biocompatible magnetic mixed micelles can be utilized in theranostic nanomedicine for targeted drug delivery system visible by MR or FL images.

Acknowledgements

The present work was supported by JSPS KAKENHI (Grant number 26248024). The neutron experiment at the Materials and Life Science Experimental Facility of the J-PARC was performed under a user program (Proposal No. 2017PM0001). The MRI experiments of this work were performed in the Division for Small Animal MRI, Medical Research Support Center, Graduate School of Medicine, Kyoto University, Japan.

References

[1] Caravan P 2006 Strategies for increasing the sensitivity of gadolinium based MRI contrast agents *Chem. Soc. Rev.* **35** 512.

[2] Zhao L, Shiino A, Qin H, Kimura T, and Komatsu N 2015 Synthesis, characterization, and magnetic resonance evaluation of polyglycerol-functionalized detonation nanodiamond conjugated with gadolinium(III) complex *J. Nanosci. Nanotechnol.* **15** 1076.

[3] Chan K W and Wong W 2007 Small molecular gadolinium(III) complexes as MRI contrast agents for diagnostic imaging *Coord. Chem. Rev.* **251** 2428.

[4] Braverman I M and Cowper S 2010 Nephrogenic systemic fibrosis *F1000 Med. Rep.* **2** 84.

[5] Davies G L, Kramberger, I and Davis J J 2013 Environmentally responsive MRI contrast agents *Chem. Commun*. **49** 9704.

[6] Reiter T, Ritter O, Prince M R, Nordbeck P, Wanner C, Nagel E and Bauer W R 2012 Minimizing risk of nephrogenic systemic fibrosis in cardiovascular magnetic resonance *J. Cardiovasc. Magn. Reson.* **14** 31.

[7] Thomsen H S, Morcos S K, Almén T, Bellin M, Bertolotto M, Bongartz G, Clement O, Leander P, Heinz-Peer G, Reimer P, Stacul F, Van der Molen A and Webb JAW 2013 Nephrogenic systemic fibrosis and gadolinium-based contrastmedia: updated ESUR contrast medium safety committee guidelines *Eur Radiol* **23** 307.

[8] Winalski C S, Shortkroff S, Mulkern R V, Schneider E, and Rosen G M 2002 Magnetic resonance relaxivity of dendrimer-linked nitroxides *Magn. Reson. Med.* **48** 965.

[9] Garmendia S, Mantione D, Castro S A, Jehanno C, Lezama L, Hedrick J L, Mecerreyes D, Salassa L, and Sardon H 2017 Polyurethane based organic macromolecular contrast agents (PU-ORCAs) for magnetic resonance imaging *Polym. Chem.* **8** 2693.

[10] Nguyen H V T, Chen Q, Paletta J T, Harvey P, Jiang Y, Zhang H, Boska M D, Ottaviani M F, Jasanoff A, Rajca A and Johnson J A 2017 Nitroxide-based macromolecular contrast agents with unprecedented transverse relaxivity and stability for magnetic resonance imaging of tumors *ACS Cent. Sci.* **3** 800.

[11] Bye N, Hutt O E, Hinton T M, Acharya D P, Waddington L J, Moffat B A, Wright D K, Wang H X, Mulet X, Muir B W 2014 Nitroxide-loaded hexosomes provide MRI contrast in vivo Langmuir 30 8898.

[12] Rajca A, Wang Y, Boska M, Paletta J T, Olankitwanit A, Swanson M A, Mitchell D G, Eaton S S, Eaton G R, and Rajca S 2012 Organic radical contrast agents for magnetic resonance imaging *J. Am. Chem. Soc.* **134** 15724.

[13] Sowers M A, McCombs J R, Wang Y, Palette J T, Morton S W, Dreaden E C, Boska M D, Ottaviani M F, Hammond P T, Rajca A and Johnson J A 2014 Redox-responsive branched-bottlebrush

polymers for in vivo MRI and fluorescence imaging *Nat. Commun*. **5** 5460.

[14] Nagura K, Takemoto Y, Moronaga S, Uchida Y, Shimono S, Shiino A, Tanigaki K, Amano T, Yoshino F, Noda Y, Koizumi S, Komatsu N, Kato T, Yamauchi J, and Tamura R 2017 Preparation of robust metal-free magnetic nanoemulsions encapsulating low-molecular-weight nitroxide radicals and hydrophobic drugs directed toward MRI-visible targeted delivery *Chem. Eur. J.* **23** 15713.

[15] Zhelev Z, Bakalova R, Aoki I, Matsumoto K, Gadjeva V, Anzaib K and Kanno I 2009 Nitroxyl radicals as low toxic spin-labels for non-invasive magnetic resonance imaging of blood–brain barrier permeability for conventional therapeutics *Chem. Commun.* 53.

[16] Emoto M C, Yamada K, Yamato M and Fujii H G 2013 Novel ascorbic acid-resistive nitroxide in a lipid emulsion: An efficient brain imaging contrast agent for MRI of small rodents *Neurosci. Lett.* **546** 11.

[17] Lu X, Zhang Z, Xia Q, Hou M, Yan C, Chen Z, Xu Y, Liu R 2018 Glucose functionalized carbon quantum dot containing organic radical for optical/MR dual-modality bioimaging *Mater. Sci. Eng. C* **82** 190.

[18] Chen C, Kang N, Xu T, Wang D, Ren L and Guo X 2015 Core–shell hybrid upconversion nanoparticles carrying stable nitroxide radicals as potential multifunctional nanoprobes for upconversion luminescence and magnetic resonance dual-modality imaging *Nanoscale* **7** 5249

[19] Kerwin B A 2008 Polysorbates 20 and 80 used in the formulation of protein biotherapeutics: structure and degradation pathways *J. Pharm. Sci.* **97** 2924.

[20] Bhattacharjee J, Verma G, Aswal V K, Date A A, Nagarsenker M S and Hassan P A 2010 Tween 80-sodium deoxycholate mixed micelles: structural characterization and application in doxorubicin delivery *J. Phys. Chem. B* **114** 16414.

[21] Strickley R G 2004 Solubilizing excipients in oral and injectable formulations *Pharm. Res.* **21** 201.

[22] Mohanty P S, Dietsch H, Rubatat L, Stradner A, Matsumoto K, Matsuoka H and Schurtenberger P 2009 Synthesis and characterization of novel functional electrosterically stabilized colloidal particles prepared by emulsion polymerization using a strongly ionized amphiphilic diblock copolymer *Langmuir* **25** 1940.

[23] Jia M, Tang Y, Lam Y F, Green S A and Blough N V 2009 Prefluorescent nitroxide probe for the highly sensitive determination of peroxyl and other radical oxidants *Anal. Chem.* **81** 8033.

[24] Chen W, Wang X, Tu X, Pei D, Zhao Y and Guo X, 2008 Water-soluble off–on spin-labeled quantum-dots conjugate *Small* **4** 759.

[25] Lozinsky E, Martin V V, Berezina T A, Shames A I, Weis A L, Likhtenshtein G I 1999 Dual fluorophore–nitroxide probes for analysis of vitamin C in biological liquids *J. Biochem. Biophys. Methods* **38** 29.

[26] Hideg E, Kalai T, Hideg K, Vass I 1998 Photoinhibition of photosynthesis in vivo results in

singlet oxygen production detection via nitroxide-induced fluorescence quenching in broad bean leaves *Biochemistry* **37** 11405.

[27] Matsuoka Y, Yamato M, Yamasaki T, Mito F, Yamada K 2012 Rapid and convenient detection of ascorbic acid using a fluorescent nitroxide switch *Free Radic. Biol. Med.* **53** 2112.

[28] Vianello F, Momo F, Scarpa M and Rigo A 1995 Kinetics of nitroxide spin label removal in biological systems: an in vitro and in vivo ESR study *Magn. Reson. Imaging* **13** 219.

[29] Levine M, Padayatty S J and Espey M G 2011 Vitamin C: a concentration-function approach yields pharmacology and therapeutic discoveries, *Adv. Nutr.* **2** 78.

[30] Yamasaki T, Mito F, Matsuoka Y, Yamato M and Yamada K, In Nitroxides - Theory, Experiment and Applications, Kokorin, A. I., Ed.; INTECH, Rijeka, Croatia, 2012; Chapter 8.

[31] Zhuang X, Xiao C, Oyaizu K, Chikushi N, Chen X and Nishide H 2010 Synthesis of amphiphilic block copolymers bearing stable nitroxyl radicals *J. Poly. Sci. Part A: Polym. Chem.* **48** 5404.

[32] Yoshitomi T, Mikyamoto D and Nagasaki Y 2009 Design of core-shell-type nanoparticles carrying stable radicals in the core *Biomacromolecules* **10** 596.

[33] Dobrynin S A, Glazachev Y I, Gatilov Y V, Chernyak E I, Salnikov G E and Kirilyuk I A 2018 Synthesis of 3,4-bis(hydroxymethyl)-2,2,5,5-tetraethylpyrrolidin-1-oxyl via 1,3-dipolar cycloaddition of azomethine ylide to activated alkene *J. Org. Chem.* **83** 5392.

[34] Kirilyuk I A, Bobko A A, Semenov S V, Komarov D A, Irtegova I G, Grigor'ev I A and Bagryanskaya E 2015 Effect of sterical shielding on the redox properties of imidazoline and imidazolidine nitroxides *J. Org. Chem.* **80** 9118.

[35] Paletta J T, Pink M, Foley B, Rajca S and Rajca A 2012 Synthesis and reduction kinetics of sterically shielded pyrrolidine nitroxides *Org. Lett.* **14** 5322.

[36] Marx L, Chiarelli R, Guiberteau T and Rassat A 2000 A comparative study of the reduction by ascorbate of 1,1,3,3-tetraethylisoindolin-2-yloxyl and of 1,1,3,3-tetramethylisoindolin-2-yloxyl *J. Chem. Soc., Perkin Trans. 1*, 1181.

[37] Muir B W, Acharya D P, Kennedy D F, Mulet X, Evans R A, Pereira S M, Wark K L, Boyd B J, Nguyen T, Hinton T M, Waddington L J, Kirby N, Wright D K, Wang H X, Egan G F and Moffat B A 2012 Metal-free and MRI visible theranostic lyotropic liquid crystal nitroxide-based nanoparticles *Biomaterials* **33** 2723.

[38] Livramento J B, Tóth E, Sour A, Borel A, Merbach A E, and Ruloff R 2005 High Relaxivity confined to a small molecular space: A metallostar-based, potential MRI contrast agent *Angew. Chem. Int. Ed.* **44** 1480.

[39] Caravan P, Farrar C T, Frullano L and Uppal R 2009 Influence of molecular parameters and increasing magnetic field strength on relaxivity of gadolinium- and manganese-based T1 contrast agents *Contrast Media Mol. Imaging* **4** 89.

[40] de Sousa P L, Livramento J B, Helm L, Merbach A E, Meme W, Doan B T, Beloeil J C, Prata M I, Santos A C, Geraldes C F and Toth E 2008 *In vivo* MRI assessment of a novel Gd^{III}-based contrast agent designed for high magnetic field applications*Contrast Media Mol. Imaging* **3** 78.

[41] Vallet P, Haverbeke Y V, Bonnet P A, Subra G, Chapat J P and Muller R N 1994 Relaxivity enhancement of low molecular weight nitroxide stable free radicals: Importance of structure and medium *Magn Reson Med.* **32** 11.